Global Journal of Pure and Applied Mathematics.
ISSN 0973-1768 Volume 22, Number 2 (2026), pp. 314-342

https://www.ripublication.com

Steady–Unsteady Comparison of Williamson Nanofluid Bioconvection over a Rotating Cone Under Porous Wall and Thermal Source/Sink Conditions

Hymavathi Dyapa
Assistant Professor, Department of Mathematics, University college of Science, Mahatma Gandhi University, Nalgonda, Telangana, India- 508254,
Email: dyapahyma@gmail.com

Abstract
The current idea compares and contrasts the unsteady incompressible mixed bioconvective of Williamson Non-Newtonian nanofluids due to the presence of cone rotation. For this inquiry, radiative flux with internal heat generation, absorption through a porous material, and bioconvection of bacteria and chemical reactions are taken into consideration. Also, along the x and y directions, velocity slip conditions are considered. Using similarity variables, the defined coupled nonlinear differential equations are converted into ordinary differential form. These coupled nonlinear equations are solved numerically using the Matlab solver and the BVP5c approach. The main outcomes of the investigations are: Δ_u risesmomentum rate of transfer of velocity profile in the y direction $g'(0)$ is increases, heat transfer rate coefficient $-\theta'(0)$ is showing mixed behaviour with increasing of heat generation/ absorption parameter Q. Mass transfer rate coefficient $-\phi'(0)$ is increasing for some time of fluid flow later it is decrease for rising for chemical reaction parameter K. The porous parameter P effects the rate of transmission of microbes $-h'(0)$is an increasing for certain time and later it is decreasing with an increasing of porous parameter P.

Keywords: Williamson fluids, Nanoliquid, Gyrotactic microorganisms, bio-convection, porous medium, heat generation or absorption, chemical reaction, velocity slip conditions.

Introduction

Since nano liquids are so intricate and diverse, they play a major role in contemporary research. They are employed in many different fields, including food processing, medicine, and the petroleum sector. First, Choi and Eastman[1]introduced the idea of nanofluid. They talked about how base fluids use nano liquids' thermal conductivity. Wang et. al[2]looked at how radiation and the build-up of nanoparticles affected the flow of nanofluid. Gowda et al.[3] computer investigation looked at Stefan blowing's impacts on second-gradient fluid. The sedimentation of thermophoretic particles in an

unstable hybrid nanofluid was investigated by Gowda et al. [4].Li et al. [5] examined entropy and the hybrid nano liquid in nonlinear mixed convective flow. Gyrotactic microorganisms and MHD Williamson nanofluid were studied by Yusuf et al. [6]. Prasannakumara [7] investigated heat transfer in Maxwell nanofluid flow quantitatively. Using the Hamilton-Crosser model, Benos et al. [8] investigated the MHD convection of CNT-Water naofluid. Large eddy simulation (LES) of turbulent and transitional channel flows of a conductive fluid under the influence of a uniform magnetic field was investigated by Sarris et al. [9]. The effectiveness of particle micro mixing in heavy metal removal procedures was examined by Karvelas et al. [10]. Gowda et al. [11], [12], [13], [14], [15] investigated the flow of nanofluids for various geometries. The Williamson fluid model [16] was created by English mathematician Williamson in 1929, and it was taken into consideration by many studies. A non-Newtonian fluid model with a shear thinning property is the Williamson fluid. The MHD Williamson Maxwell nanofluid across a sheet was studied by Abdal et al.[17]. Williamson nanofluid flow was examined for radiation and velocity slip by Qayyum et al. [18].The Fick's and Fourier's notion for heat production in nonlinear convective Williamson nanofluid flow was examined by Waqas et al.[19]. Chu et al.'s research[20], [21] used chemical reactions and activation energy to examine the thermal energy of hybrid nanoparticles. He went into detail about the effects of convective boundary conditions, heat generation, and the characteristics of thermal radiation. Numerous researchers have completed similar studies [22], [23], [24]. Thermal radiation is used in nuclear power plants, gas turbines, and a variety of engineering applications, including propulsion systems for satellites, aircraft, and spacecraft. Consequently, a lot of research has focused on how radiative heat transmission affects nanofluids. Regarding this, Elbashbeshy et. al. [25] talked about free heat convection and boundary layer fluid flow around a thermal sphere through a porous material when thermal radiation and pressure stress work are present. Furthermore, the impact of radiation and pressure gradient on nonlinear boundary layer fluid flow across a flat plate was examined by Xenos et al. [26].Due to the emergence of new species, the chemical reaction in nanofluid flow has a significant impact on transport phenomena, which in turn influences production criteria. There are numerous researchers looking into these consequences. The impact of reactive species on unstable convective heat and mass transfer in fluid flow caused by a stretching plate in porous media was examined by Chamkha and Mansour [27]. The impact of forced convection on mass and heat transfer in nanofluid flow through a porous channel with a chemical reaction occurring on the wall was documented by Matin and Pop [28]. Zang et.al [29] took into account the changing heat flux while analysing the effects of radiative heat and chemical reactions on the flow of MHD nanofluid across a flat plate through porous media. The effects of thermal radiation and chemical reaction on mixed convection heat and mass transfer in nanofluid flow over a stretching sheet in a porous media were investigated by Pal and Mandal [30]. There are various applications of bioconvection in the fields of biotechnology and natural systems. To study fluid behaviour, scientists use the bioconvection of living microorganisms. Maxwell nanofluid including gyrotactic organisms and nonlinear thermal radiation was studied by Ramesh et al. [31]. In addition to uses of modified

Darcy law, Song et al. [32] described the micropolar nanofluid for nonlinear thermal radiation having gyrotactic organism's flow. The gyrotactic analysis of a Sutter by nanofluid with several thermal properties was investigated by Farooq et al.[33].

This review of previous research indicates that there is little discussion of the bio-convection of microorganisms submerged in Williamson nanofluid flowing around a spinning cone. The physical characteristics of this study are enhanced by the nanofluid flow across the cone's slip surface through porous walls in the presence of heat radiation and a magnetic field including Chemical reaction. There appears to be a void to fill:

1) The effect of flow across a revolving through porous walls of Cone on the distribution of nanoparticles.
2) What is the impact of steady and unsteady fluid flow with Chemical reaction, heat generation/absorption, heat radiation, and magnetic field, and bio-convection on Williamson nanofluid slip transportation?

The goal of this effort is to improve thermal distribution by adding porous walls of Cone, and fluid with nano-entities, which will raise the base fluid's thermal conductivity. The concern regarding the potential settling of nanomaterials is undermined by microbe density gradients. Therefore, in addition to nanofluid transmission over the cone, bioconvection with Wu's slip conditions and heat generation / absorption are taken into account. In rotational dynamical systems, certain physical features involving heat and mass flow over cone geometry are feasible. The findings have potential uses in the effective operation of transfer engines, microelectronic cooling, and heat exchangers.

Mathematical Formulation

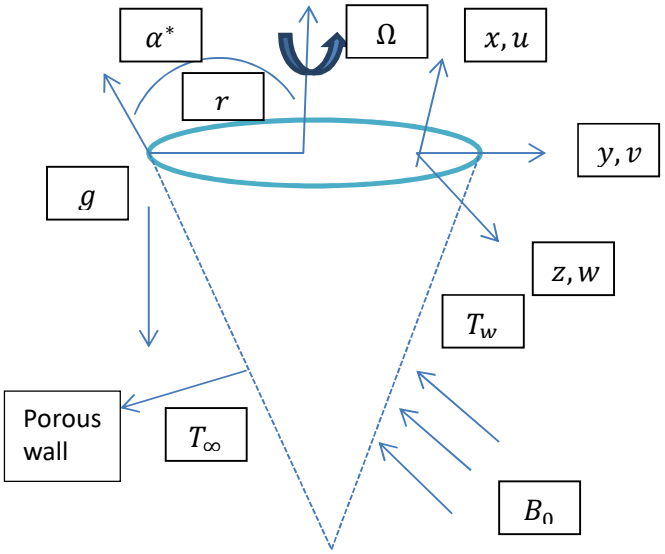

Figure 1. Geometry of flow analysis

Because of Wu's slip conditions, the fluid flowing past a rotating porous cone incorporating microorganisms is thought to be an unstable, laminar, incompressible mixed convection of Williamson nano liquid with internal heat generation and absorption, thermal radiation, and chemical reaction. Cone rotation velocity as a function of time is assumed, which leads to flow field instability. The buoyant forces in the flow field are caused by differences in mass, temperature, and microbes. Components of velocityu, v and w are in tandem with $x, y$and$z$instructions. The representation of cone spinning in a porous media is $\boldsymbol{\Omega}$ (see Fig. 1). Slips in flow velocity are taken into$x$ and y directions. StrengthB_0magnetic field acting perpendicular to the x- axis. The cone half angle isα^*. The self-motile microorganisms are dilute mixed with base fluid. The motion of microorganisms does not depend on the transport of nano liquid particles and vice versa. The temperature, nano particle concentration and microorganisms have constant wall conditions. The Hall effect is taken into account. The leading equations' formulation is shown as[34], [35], [36], [37], [38], [39], [40]

$$\frac{\partial(xu)}{\partial x}+\frac{\partial(xw)}{\partial z}=0 \tag{1}$$

$$\frac{\partial u}{\partial t}+u\frac{\partial u}{\partial x}-\frac{v^2}{x}+w\frac{\partial u}{\partial z}=\nu_0\left(\frac{\partial^2 u}{\partial z^2}+\sqrt{2}\Gamma\frac{\partial u}{\partial z}\frac{\partial^2 u}{\partial z^2}\right)-\frac{\sigma B_0^2(u+mv)}{\rho(1+m^2)}+\frac{1}{\rho}\Big(\beta_M(1-C_\infty)\rho g(T-T_\infty)-g\big(\rho_p-\rho\big)(C-C_\infty)-(n-n_\infty)g\gamma(\rho_m-\rho)\Big)-\frac{\gamma}{K_0}u \tag{2}$$

$$\frac{\partial v}{\partial t}+u\frac{\partial v}{\partial x}+\frac{uv}{x}+w\frac{\partial v}{\partial z}=\nu_0\left(\frac{\partial^2 u}{\partial z^2}+\sqrt{2}\Gamma\frac{\partial u}{\partial z}\frac{\partial^2 u}{\partial z^2}\right)-\frac{\sigma B_0^2(u+mv)}{\rho(1+m^2)}-\frac{\gamma}{K_0}u \tag{3}$$

$$\frac{\partial T}{\partial t}+u\frac{\partial T}{\partial x}+w\frac{\partial T}{\partial z}=\frac{k}{\rho c_p}\frac{\partial^2 T}{\partial z^2}+\frac{\mu}{\rho c_p}\left(\left(\frac{\partial u}{\partial z}\right)^2+\left(\frac{\partial v}{\partial z}\right)^2\right)+\frac{16T_\infty^3\sigma^*}{3k^*K}\frac{\partial}{\partial z}\frac{\partial T}{\partial z}+\frac{\sigma B_0^2(u^2+v^2)}{\rho c_p}+\tau D_B\frac{\partial C}{\partial z}\frac{\partial T}{\partial z}\tau\frac{D_T}{T_\infty}\left(\frac{\partial T}{\partial z}\right)^2+\frac{Q_0}{\rho c_p}(T-T_\infty) \tag{4}$$

$$\frac{\partial C}{\partial t}+u\frac{\partial C}{\partial x}+w\frac{\partial C}{\partial z}=D_B\frac{\partial^2 C}{\partial z^2}+\frac{D_T}{T_\infty}\frac{\partial^2 T}{\partial z^2}-K_r(C-C_\infty) \tag{5}$$

$$\frac{\partial n}{\partial t}+u\frac{\partial n}{\partial x}+w\frac{\partial n}{\partial z}+\frac{b_c W_c}{C_{w-C_\infty}}\left(\frac{\partial}{\partial z}\left(n\frac{\partial C}{\partial z}\right)\right)=D_n\frac{\partial^2 n}{\partial z^2} \tag{6}$$

Under suitable boundary conditions

$$u=N_0\mu\frac{\partial u}{\partial z},\ v=\frac{\Omega sin\alpha^*}{1-qt^*}+N_0\mu\frac{\partial v}{\partial z},\ w=0, T=T_w, C=C_w, n=n_w,\ \text{at}\ \eta=0$$

$$u=0,\ v=0,\ T=T_\infty,\ C=C_\infty,\ n=n_\infty \qquad \eta\to\infty \tag{7}$$

Here, the indicated similarity transformations are applied to obtain the necessary system of ordinary differential equations.

$$u=\frac{-\Omega xsin\alpha^*}{2(1-qt^*)}f'(\eta),\ v=\frac{\Omega xsin\alpha^*}{(1-qt^*)}\,g(\eta),\ w=\sqrt{\frac{\nu_0\Omega sin\alpha^*}{(1-qt^*)}}\,f(\eta),\ \theta(\eta)=\frac{T-T_\infty}{T_w-T_\infty},$$

$$T_w-T_\infty=\frac{x(T_0-T_\infty)}{L(1-qt^*)^2},\ \emptyset(\eta)=\frac{C-C_\infty}{C_w-C_\infty},\ C_w-C_\infty=\frac{x(C_0-C_\infty)}{L(1-qt^*)^2}h(\eta)=\frac{n-n_\infty}{n_w-n_\infty},$$

$$n_w-n_\infty=\frac{x(n_0-C_\infty)}{L(1-qt^*)^2},\qquad t^*=(\Omega sin\alpha^*)t,\qquad \eta=z\sqrt{\frac{\Omega sin\alpha^*}{\nu_0(1-qt^*)}} \tag{8}$$

The system of ordinary differential equations that was obtained is as follows.

$$f'''(1-\beta f'')+\frac{f'^2}{2}-2g^2-ff''-S\left(f'+\frac{\eta}{2}f''\right)-2\lambda(\theta-Nr\phi-Rbh)-\frac{M}{1+m^2}(f'-2mg)-Pf'=0 \quad (9)$$

$$g''(1+\beta g')+gf'-fg'-S\left(g+\frac{\eta}{2}g'\right)-\frac{M}{1+m^2}\left(\frac{mf'}{2}+g\right)-Pg=0 \quad (10)$$

$$(1+R)\theta''-Pr\left(S\left(2\theta+\frac{\eta}{2}\theta'\right)-\frac{f'\theta}{2}+f\theta'\right)+PrEc\left(\frac{f''^2}{4}+g'^2\right)+MPrEc\left(\frac{f'^2}{4}+g^2\right)+Nb\theta'\phi'+Nt\theta''+Q\theta=0 \quad (11)$$

$$\phi''-Sc\left(S\left(2\phi+\frac{\eta}{2}\phi'\right)-\frac{f'\phi}{2}+f\phi'\right)+\frac{Nt}{Nb}\theta''-K\theta=0 \quad (12)$$

$$h''-Lb\left(S\left(2h+\frac{\eta}{2}h'\right)-\frac{f'h}{2}+fh'\right)+Pe[\phi''(h+\delta)+h'\phi']=0 \quad (13)$$

Appropriate boundary conditions that have been transformed are:

$f(0)=0,\ f'(0)=\Delta_u f''(0),\ g(0)=1+\Delta_u g'(0),\ \theta(0)=1,\ \phi(0)=1,\ h(0)=1\ at\ \eta=0$ and

$f'(\infty)\to 0,\ g(\infty)\to 0,\ \theta(\infty)\to 0,\ \phi(\infty)\to 0,\ h(\infty)\to 0\ as\ \eta\to\infty$ 14)

The parameters that are nondimensional are

$\to \beta=\Gamma x\sqrt{\frac{1}{2\nu_0}\left(\frac{\Omega sin\alpha^*}{1-qt^*}\right)^3}$ Williamson fluid parameter,

$\to M=\frac{\sigma B_0^2(1-qt^*)}{\rho\Omega sin\alpha^*}$Magnetic parameter

$\to Nr=\frac{(\rho_p-\rho)(C-C_\infty)}{\rho\beta_M(1-C_\infty)(T-T_\infty)}$ Buoyancy ratio parameter

$\to Rb=\frac{\gamma(\rho_m-\rho)(n-n_\infty)}{\rho\beta_M(1-C_\infty)(T-T_\infty)}$ Rayleigh number

$\to \lambda=\frac{Gr}{Re^2}$ Mixed convection parameter

$\to Gr=\frac{g\beta_t cos\alpha^*(T-T_\infty)L^3}{\nu_0^2}$ Grashof number

$\to Re=\frac{L^2\Omega sin\alpha^*}{\nu_0}$ Reynolds number

$\to Sc=\frac{\nu}{D_B}$ Schmidt number

$\to Pr=\frac{k}{\alpha}$ Prandtl number

$\to R=\frac{16T_\infty^3\sigma^*}{3k^*K}$ Radiation parameter

$\to Pe=\frac{b_c W_c}{\nu_0}$ Peclet number

$\to Lb=\frac{\nu}{D_m}$ Bio convection Lewis number

$\to Nb=\frac{\tau D_B(C-C_\infty)(T-T_\infty)}{L(1-qt^*)^2}$ Brownian motion parameter

$\to Nt=\frac{\tau D_T(T-T_\infty)\Omega sin\alpha^*}{T_\infty(1-qt^*)^2L\nu_0}$ Thermophoresis parameter

Additional dimensionless physical quantities

Skin friction coefficient

The following represents the coefficient of surface drag:

$Cf_x = \frac{2\tau_{xz}}{\rho\left(\frac{\Omega sin\alpha^*}{1-qt^*}\right)^2}$

Where, τ_{xz} is a shear stress detector and is defined as:

$\tau_{xz} = \mu(1+\beta)\left(1+\frac{\Gamma}{2}\frac{\partial u}{\partial z}\right)\frac{\partial u}{\partial z} \;\; at\; z = 0$

The dimensionless formulation of the previous problem is obtained by applying Eq. (8):

$Cf_x(Re_x)^{\frac{1}{2}} = -\left(f''(0) + \beta\left(f''(0)\right)^2\right)$

Also

$Cf_y = \frac{2\tau_{yz}}{\rho\left(\frac{\Omega sin\alpha^*}{1-qt^*}\right)^2}$where, τ_{yz} is a shear stress detector and is defined as:

$\tau_{yz} = \mu(1+\beta)\left(1+\frac{\Gamma}{2}\frac{\partial v}{\partial z}\right)\frac{\partial v}{\partial z} \;\; at \;\; z = 0$

Applying Eq. (8) the dimensionless formulation of the preceding equation is:

$Cf_y(Re_x)^{\frac{1}{2}} = -\left(g'(0) + \beta\left(g'(0)\right)^2\right)$

Local Nusselt number. The mathematical solution for the heat transfer efficiency relationship is as described in the following:

$Nu_x = \frac{xq_w}{k(T_w - T_\infty)}$ the external heat transfer is:

$q_w = -\frac{\partial T}{\partial z} - \frac{16T_\infty^3\sigma^*}{3k^*}\frac{\partial T}{\partial z} \;\; at \;\; z = 0$

Using Eq. (8) the preceding solution is reduced as follows:

$Nu_x(Re_x)^{-1/2} = -(1-R)\theta'(0)$

Sherwood number it is defined as:

$Sh_x = \frac{xq_m}{k(C_w - C_\infty)}$

Where q_m stands for surface mass flow and is denoted as:

$q_m = -D_B\frac{\partial C}{\partial z} \;\; at \;\; z = 0$

Using Eq. (8), the above equation's non- dimensional version is:

$Sh_x(Re_x)^{-1/2} = -\phi'(0)$

Density of micro-organisms it is defined as:

$Nn_x = \frac{xq_n}{k(n - n_\infty)}$

Where q_n identifies the flux of motile micro-organisms and is delineated as:

$q_n = -D_n C\frac{\partial n}{\partial z} \;\; at \;\; z = 0$

Using Eq. (8), the non- dimensional form of equation is:

$Nn_x(Re_x)^{-1/2} = -h'(0)$

Numerical Procedure

The numerical method for the leading ordinary differential equations (9)–(13) with boundary conditions (14) is covered in this section. Analytically solving such kinds of boundary value problems is challenging. While there are other numerical techniques being employed for this, the Bvp5c method is still widely used [41], [42]. Additionally, we used the Bvp5c approach to solve the issue. The governing equations (9)–(14) are transformed into a first-order differential form as follows in order to implement this strategy:

$$f(\eta) = f(1)$$
$$f' = f'(1) = f(2)$$
$$f'(2) = f(3)$$
$$f'(3) = -\frac{1}{(1-\beta f'')}\left[\frac{1}{2}f'^{2} - ff'' - 2g^{2} - S\left(f' + \frac{1}{2}\eta f''\right) - \frac{M}{1+m^{2}}(f' - 2mg) - 2\lambda(\theta - Nr\phi - Rbh)\right] - Pf'$$
$$g(\eta) = f(4)$$
$$g'(\eta) = f'(4) = f(5)$$
$$f'(5) = \frac{-1}{(1-\beta g')}\left[-fg' + f'g - S\left(g + \frac{1}{2}\eta g'\right) - \frac{M}{1+m^{2}}\left(g + \frac{mf'}{2}\right)\right] - Pg$$
$$\theta(\eta) = f(6)$$
$$f'(6) = f(7)$$
$$f'(7) = \frac{-1}{1+R}\left[-Pr\left(f\theta' - \frac{1}{2}f'\theta + S\left(2\theta + \frac{1}{2}\eta\theta'\right)\right) + PrEc\left(\frac{f''^{2}}{4} + g'^{2}\right) + MPrEc\left(\frac{f'^{2}}{4} + g^{2}\right) + Nb\theta' + Nt\theta'^{2}\phi' - Q\theta\right]$$
$$\phi(\eta) = f(8)$$
$$f'(8) = f(9)$$
$$f'(9) = Sc\left[f\phi' - \frac{1}{2}f'\phi + S\left(2\phi + \frac{1}{2}\eta\phi'\right)\right] - \left(\frac{Nt}{Nb}\right)\theta'' - K\phi$$
$$h(\eta) = f(10)$$
$$f'(10) = f(11)$$
$$f'(11) = Lb\left[fh' - \frac{1}{2}f'h + S\left(2h + \frac{1}{2}\eta h'\right)\right] - Pe[h'\phi' + \phi''(h+\delta)]$$

With suitable transformed boundary conditions

$f(0) = 0,\ f'(0) = \Delta_u f''(0),\ -\Delta_u g'(0) + g(0) = 1, \theta(0) = 1, \phi(0) = 1, h(0) = 1\ at\ \eta = 0$ and

$f'(\infty) \to 0,\ g(\infty) = 0\ , \theta(\infty) = 0\ ,\ \phi(\infty) = 0\ ,\ h(\infty) = 0\ as\ \eta \to \infty$

With the above transformed first order ordinary differential equations are coded with help of Matlab software.

Results and Discussion

Finding the velocity profile, temperature, concentration, and density of motile microorganisms in non-Newtonian fluid profiles for the appropriate range of specified physical parameters is the first step in the computational procedure. Additionally, the computational results are analysed and their physical interpretation is explained through the diagrams and numerical comparison shown in a good argument in tolerance of the boundary conditions for the fixed values of $M = 0.5,\ \beta = 0.1, m = 0.1,\ \lambda = 0.1, Nr = 0.1, Rb = 0.1, \Delta_u = 1.0, Ec = 0.1, Nb = 0.1, Nt = 0.1, Pr = 6.2, R = 0.1, Sc = 0.2, Lb = 0.2, Pe = 1.0.\ P = 0.1$ and so the computing process is carried out, validating numerical values through tables.

It should be noted that throughout the graphs, Newtonian fluid flow is represented by breaking lines, non-Newtonian liquid flow for steady and unsteady cases are represented by solid lines, and dotted lines respectively.

The impact of Williamson parameterβon the momentum profiles in the $x\ and\ y$ directions aredisplayed in Figures 1 (a) and 1(b) respectively. When the value of βincreases, velocity in the x direction is increased whereas the decreasing behaviour is shown in the$y$ direction respectively. The temporal relaxation variable Γ and the Williamson fluid parameter β are intimately correlated, which causes flows to be retarded in y direction.

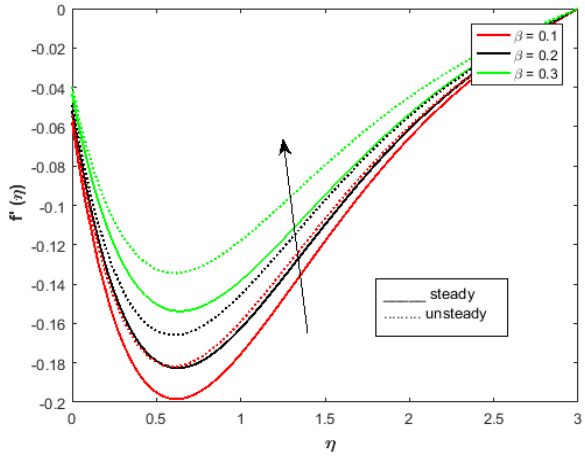

Fig. 1(a) momentum profile in the X direction V/s β

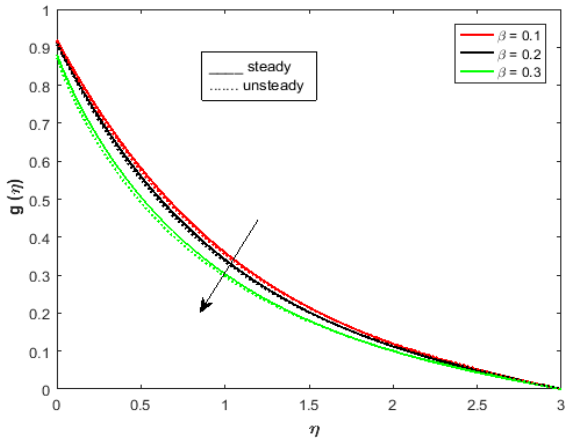

Fig. 1 (b) momentum profile in the y direction V/s β

Figures 2, which depict the behaviour of the mixed convection parameterλ on the velocity profile, demonstrate that velocity fall down initially later the momentum layer is rises with increasing λin both steady and unsteady circumstances. Because of buoyant forces, this increased mixed convection creates a mixed flow motion. The fundamental characteristic of this increase in the velocity profile is that the fluid's velocity increases as λtakes bigger values.

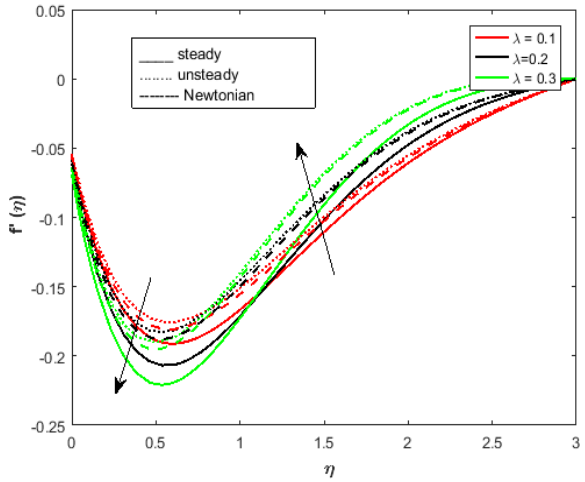

Fig. 2. momentum profile V/s λ

The velocity profile in Figures 3 (a) - 3(d), illustrates the increasing behaviour as the buoyancy ratio parametersNr, the Rayleigh number Rb, and velocity distribution parameter m increase, respectively. With higher values of these parameters, there is more resistance to fluid flow in the horizontal direction, which are the fundamental phenomena causing this acceleration in velocity profiles in the x direction respectively.

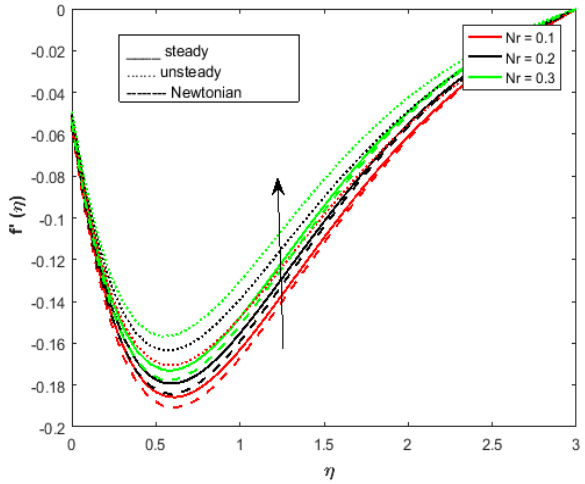

Fig. 3(a). Momentum profile V/s Nr

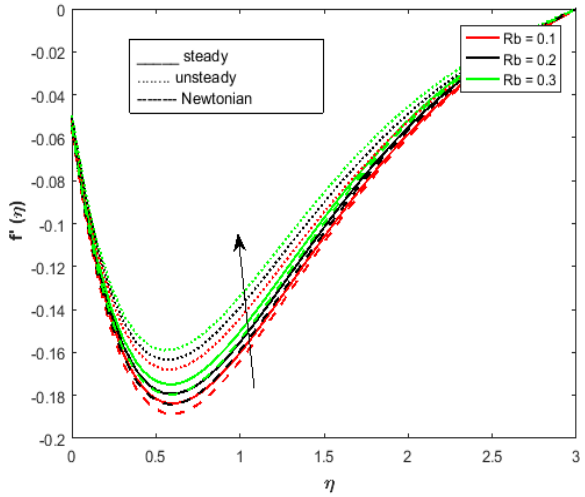

Fig. 3(b). Momentum profile V/s Rb

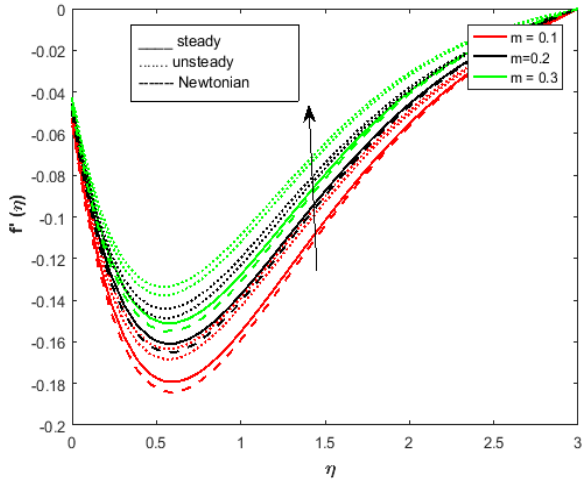

Fig. 3(c). momentum profile V/s m in the X direction

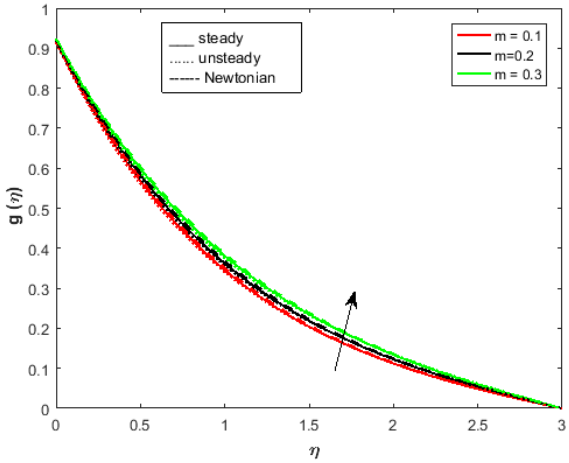

Fig. 3(d). momentum profile V/s m in the Y direction

Figures 4 (a) – 4 (f) illustrates how $\beta, P, and\ \Delta_u$affect momentum profiles in the $x\ and\ y$ direction so the skin friction changes with the non-dimensional physical parameter Williamson parameterβ, porous parameter$P$ and slip velocity parameter Δ_u. It is evident from the figures that velocity grow slightly, at a point of spot the motion of the fluid is getting up gradually toward the boundary as the values of the aforementioned non-dimensional components grow in x direction. Whereas the opposite tendency is observed for momentum profile in the y direction.

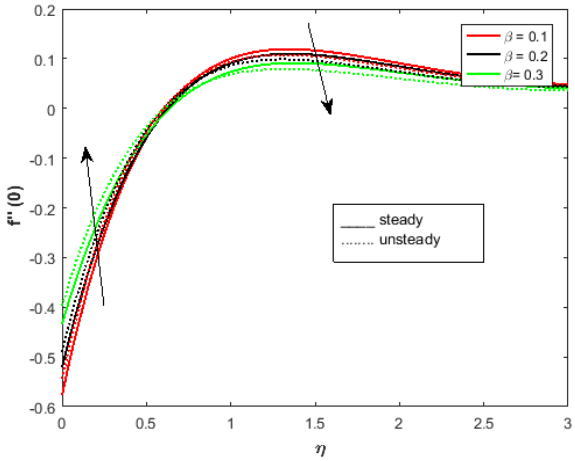

Fig. 4(a). Williamson parameter βV/s $f''(0)$

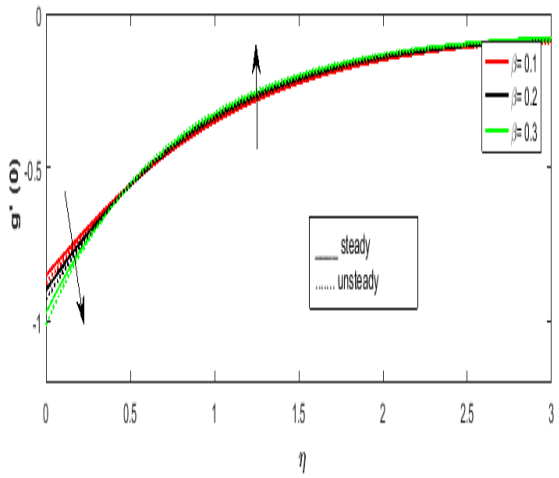

Fig. 4(b). Williamson parameter β V/s$g'(0)$

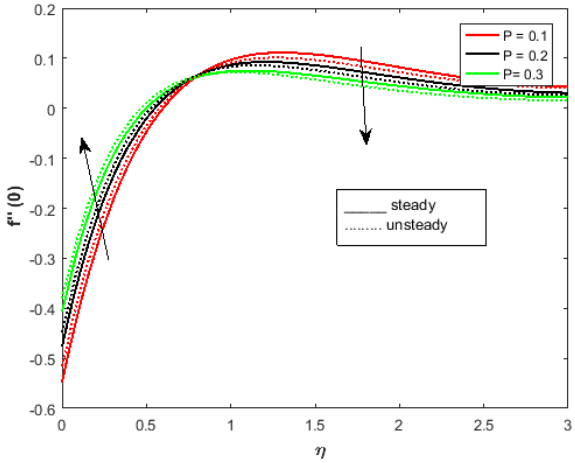

Fig. 4(c). Porous parameter P V/s $f''(0)$

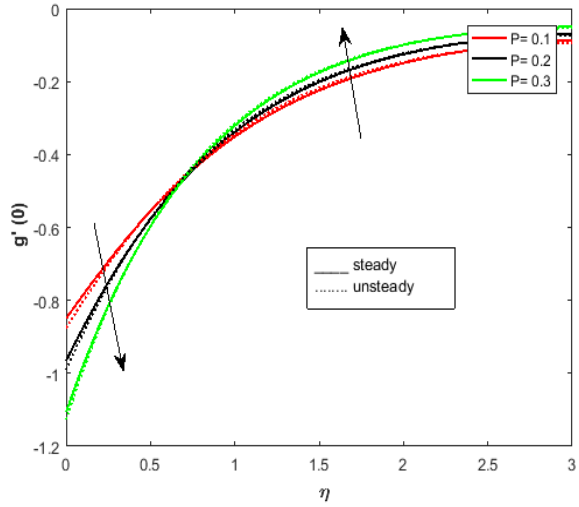

Fig. 4(d). Porous parameter P V/s $g'(0)$

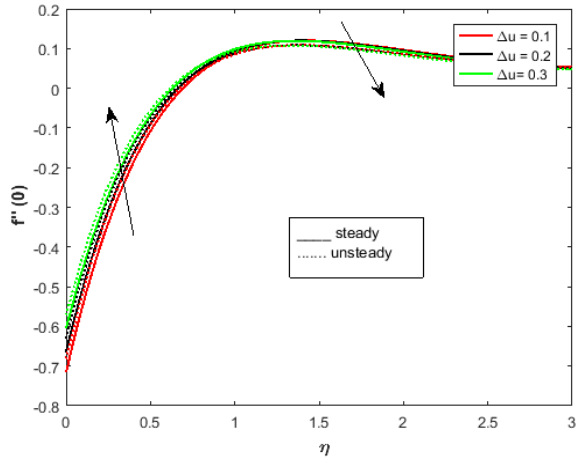

Fig. 4(e). velocity ratio parameter Δ_u V/s $f''(0)$

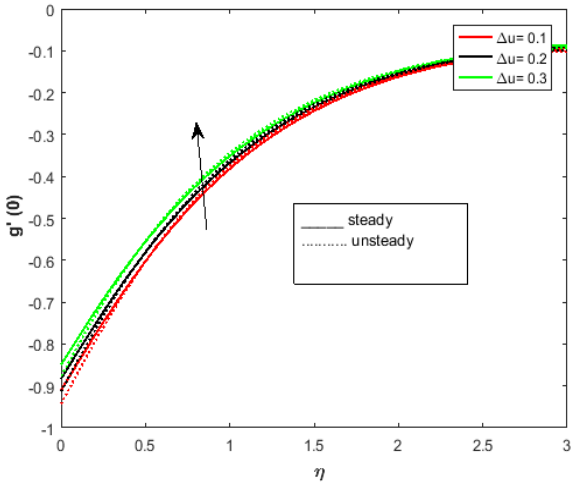

Fig. 4(f). velocity ratio parameter Δ_u V/s$g'(0)$

The influence of $Pr, Nb, Nt, Ec, and\ Q$ on the thermal profile is depicted in Figures 5(a) – 5(e).Figures demonstrate that temperature rises as $Nb, Nt, R, Ec, and\ Q$ values riseand drop down for rise in the Prandtlnumber Pr. The temperature drops when Prandtl number Pr values rise, as seen in Figure 5a. The physical relationship between Pr and thermal diffusivity, which lowers temperature in fluid. The behaviour of Brownian motion parameterNb andthermophoresis parameterNt on a temperature profile is depicted in Figures 5 (b) -5(c). It is evident from the figure that temperature increases as Nb and Nt values climb. The fundamental idea behind the rise in temperature caused by Brownian motion is that because nanoparticles and temperature are intimately correlated, an increase in temperature results in an increase in the kinetic energy of these particles. Additionally, particles migrate from hotter to colder surfaces for the thermophoresis parameter, raising the fluid's temperature. As its kinetic energy is transformed into thermal energy, raising the fluid's temperature, for higher estimations, the fluid's thermal field is physically increased by the Eckert numberEc. As a result, there is less thermal conduction into the fluid hence from figure 5 (d) it is evident that the temperature profile is increasing with rise in Ec number. The impact of heat generation/ absorption on the temperature profile is depicted in Figure 5 (e). It has been observed that as Q increases, temperature rises as well. The primary cause of this is that the radiation process generates a lot of heat and for heat generation/ absorption values $-\theta'(0)$ presented in the figures 6 (a) and 6 (b) for both cases steady and unsteady $-\theta'(0)$ profile changes inversely for heat generation (positive) and heat absorption (negative) values.

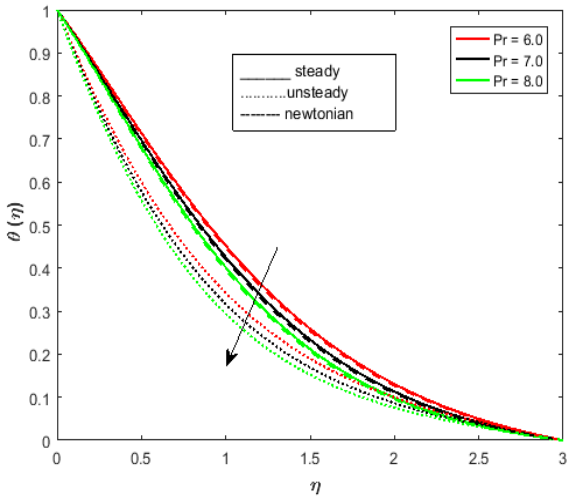

Fig.5(a). Temperature profile V/s Pr

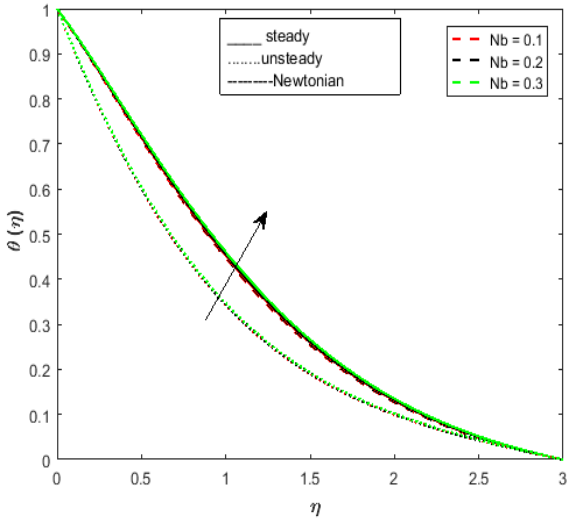

Fig.5(b). Temperature profiles V/s Nb

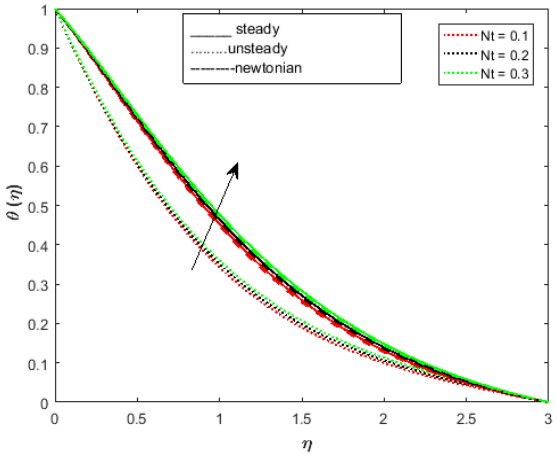

Fig. 5(c) Temperature profiles V/s Nt

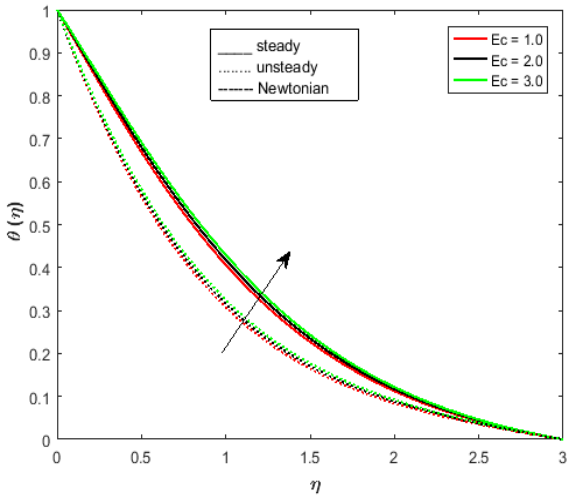

Fig. 5(d) Temperature profile V/s Ec

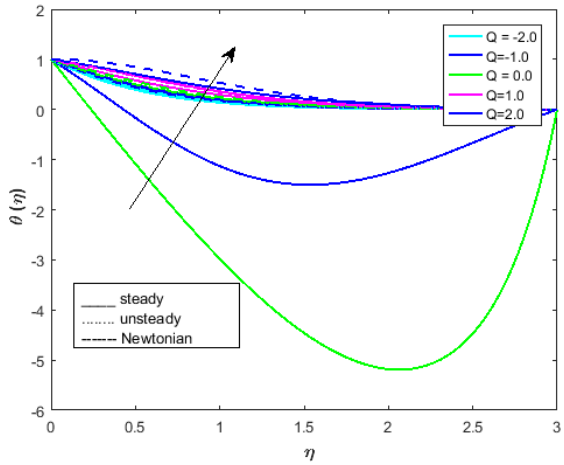

Fig. 5(e) Temperature profile V/s Q

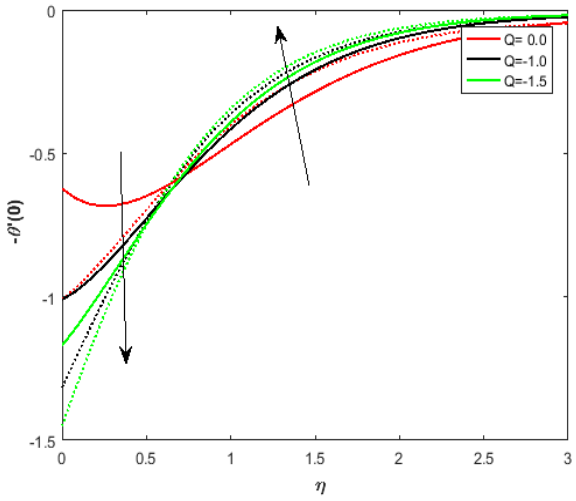

Fig. 6(a). heat absorption effects V/s $-\theta'(0)$

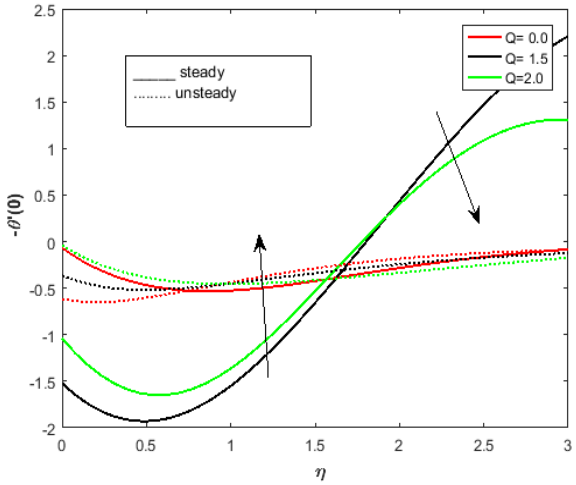

Fig. 6(b). heat generation effects V/s $-\theta'(0)$

The impact of $Nb, Nt, Sc, and\ K$ on the concentration profile is depicted in Figure 7 (a)- 7 (e). The concentration rises quickly for increasing of thermophoresis parameter Nt, and chemical reaction parameter$K$values while falling for increasing Nb and Sc values. $-\phi'(0)$show the influence for chemical reaction parameter K rises in both cases steady and unsteady cases, $-\phi'(0)$ increases initially and after some point it grows up gradually.

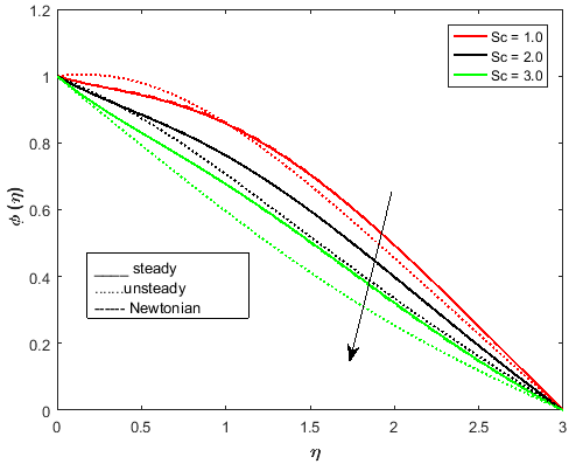

Fig. 7 (a) Schimidt number *Sc* V/s Concentration Profile

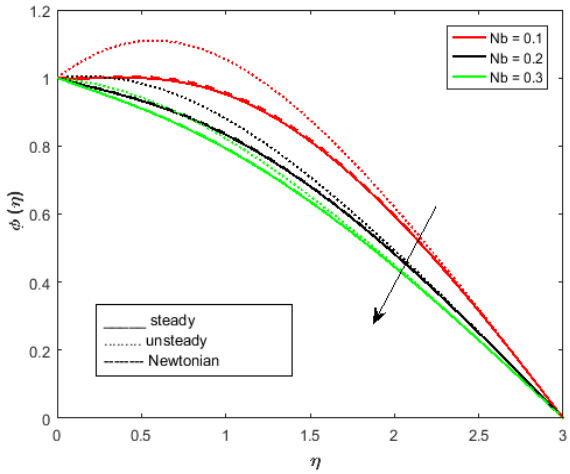

Fig. 7 (b) Brownian motion parameter *Nb* V/s Concentration Profile

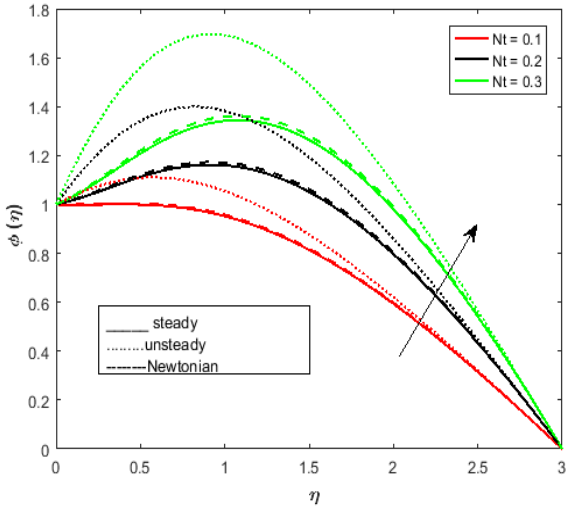

Fig. 7 (c) Thermophoresis parameter N*t* V/s Concentration Profile

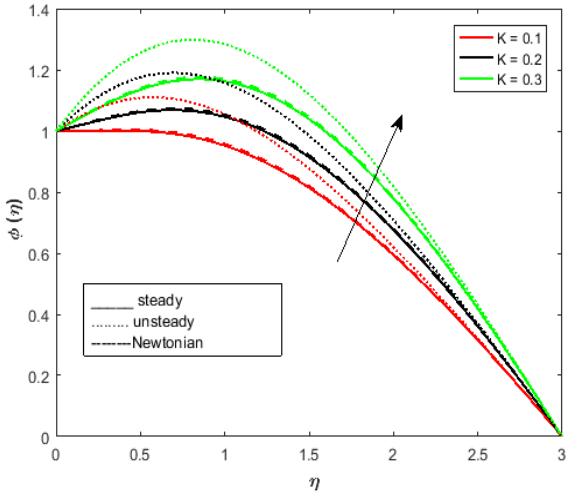

Fig. 7(d) Chemical reaction parameter *K* V/s Concentration Profile

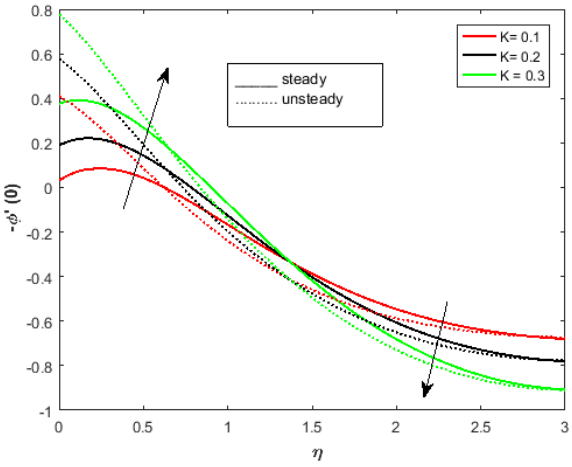

Figure 7 (e) Chemical reaction parameter K V/s $-\phi'(0)$

The impact of Lewis number Lb, Peclet number Pe and microorganism's concentration difference parameter δ on the motile density profile is displayed for both cases steady and unsteady cases in Figures 8 (a) – 8(d). It is evident that when the values of Lb, Pe, and δ increase, the motile microorganisms file decreases. The diffusivity of living microbes decreases as the Peclet number increases, which is the fundamental cause of this Pe retardation. The rate of change of motile density $-h'(0)$ of microorganisms is increase initially and at some point the motile rate of change of density of microbes is decreasing gradually.

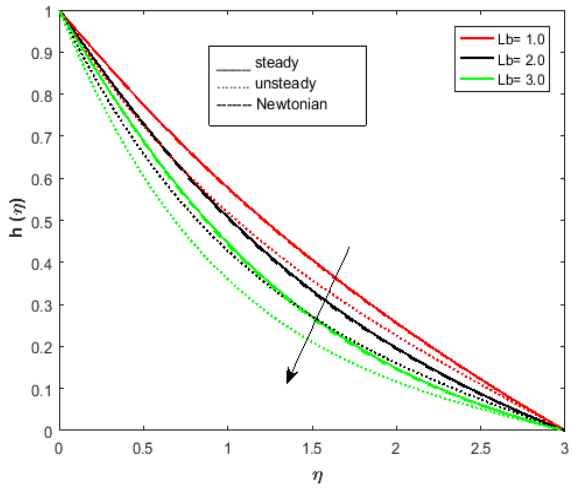

Fig. 8(a). Motile Microorganism's profile V/s Lb

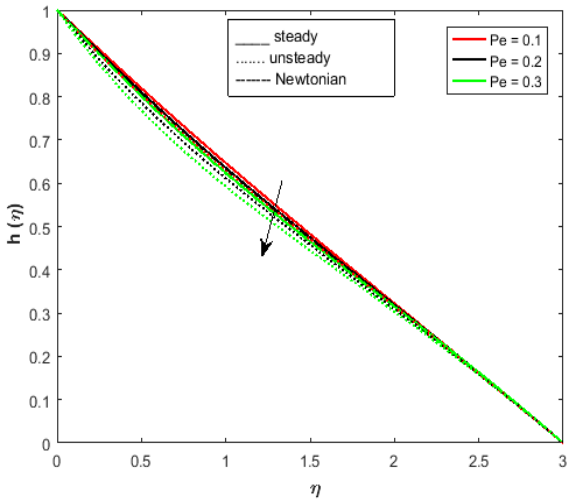

Fig. 8(b) Motile Microorganism's profile V/s Pe,

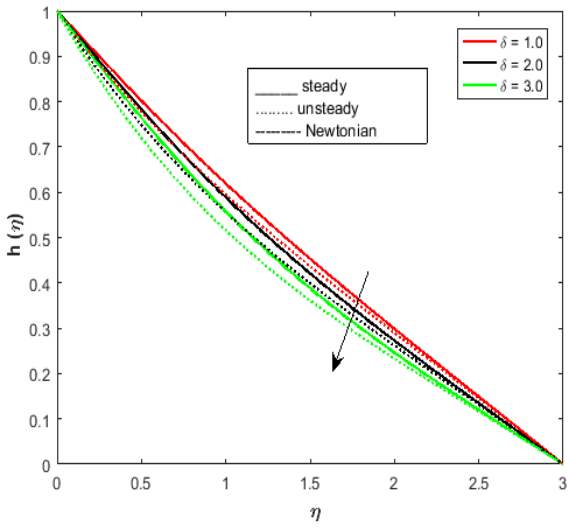

Fig.8(c). Motile Microorganism's profile V/s δ

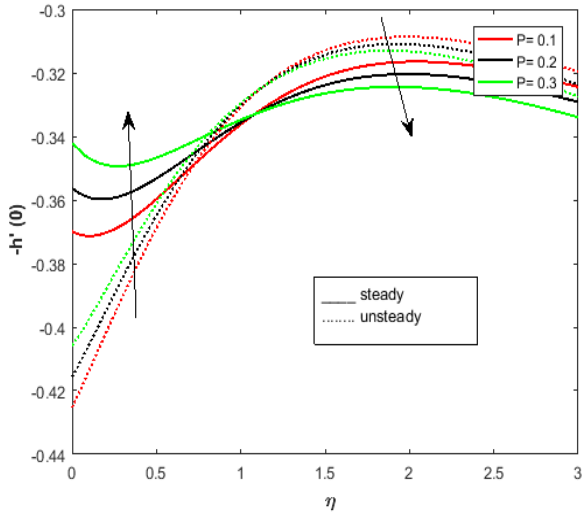

Fig. 8(d). Influence of Porous parameter P V/s$-h'(0)$

Computational study

Table 1 shows the impact of the skin friction factor for both steady and unsteady scenarios owing to various parameters such as $M, \beta, m, \lambda, Nr, Rb,\ P\ and\ \Delta_u$. The skin friction factor grows more for stable case values as M rises than for values in unsteady case. Steady cases decline more than unsteady cases when βvalue rises. The steady example exhibits greater value gain as m increases than the unsteady case. Steady case values rise higher than unsteady case values when λincreases. The values of the steady case and unsteady case both fall with an increase in Nr, but the steady case has a greater decline. There is an equivalent amount of value drop in both scenarios for every increment in Rb. When it comes to $\Delta_u$values, both case values rise in tandem withΔ_u. Coming to the Porous effect on skin friction factor $f''(0)$ rises more with rising of steady and unsteady cases. The findings of$g'(0)$ for $M, \beta, m,\ P\ and\ \Delta_u$ for both the steady and unsteady instances are displayed in Table 2. It is evident that the values of the steady case increase more than the values of the unsteady case as M increases. Conversely, a rise in $\beta,\ P$, and $\Delta_u$values result in a greater fall in steady and unsteady case values. The results for $\theta'(0)$ while $R, Nb, Nt,\ and\ Q$ are active for both instances are shown in Table 3. It is observed that in shaky circumstances, R increases more than in steady cases. On the other hand, in unstable circumstances relative to steady cases, the values of Nb, Nt, and Q heat generation decline more. Table 4 displays the effect of the Sherwood number for the various parameters K, Nb, Nt. The Sherwood number increases as Sc and Nb values rise. The unsteady scenario experiences a greater decrease with increasing Nt value than the steady case. When Γgrows, the steady case increases more than the unsteady case. Table 5 displays the $\delta, Pe, and\ Lb$ values for $h'(0)$. The values for unsteady cases increase more than those for steady cases when Lb, Pe,and δ values rise.

Table 1. Results of skin friction factor $-f''(0)$ in x- direction for various parameters

M	β	m	λ	Nr	Rb	Δ_u	P	$Stady\ case$	$Unsteady\ case$
1.0	0.5	1.0	0.1	0.1	0.1	0.1	0.1		
1.5								0.3660	0.3254
2.0								0.4156	0.4007
2.5								0.4724	0.4511
	0.5							0.4724	0.3026
	1.0							0.3178	0.2516
	1.5							0.2648	0.2308
		1.0						0.3500	0.4511
		1.5						0.4724	0.5297
		1.0						0.5152	0.5411
			0.1					0.4724	0.4889
			0.2					0.5152	0.4651
			0.3					0.5556	0.4511
				0.1				0.4724	0.4419
				0.3				0.4636	0.4326
				0.5				0.4549	0.4224
					0.1			0.4724	0.4724
					0.3			0.4584	0.4584
					0.5			0.4443	1.4443
						0.1		1.4834	1.4834
						0.5		0.4829	0.4829
						1.0		0.4724	0.4724
							0.1	0.3541	0.4611
							0.2	0.4825	0.5397
							0.3	0.6632	0.6451

Table 2. Results of Skin friction factor $g'(0)$ in y – direction for various parameters

.

M	β	P	Δ_u	$Steady\ case$	$Unsteady\ case$
1.0	0.5	1.0	1.0	1.1563	0.1298
1.5				1.2816	0.2564
2.0				1.3628	0.3231
	0.5			1.3128	1.3111
	1.0			0.9546	0.9587
	1.5			0.8456	0.8235
		0.1		1.3456	1.3864
		0.2		1.3153	1.3456
		0.3		1.2956	1.2687
			0.1	2.0869	2.0154
			0.5	1.6397	1.6307
			1.0	1.3768	1.3124

Table 3. Results of Nusselt number $-\theta'(0)$ for various parameters

R	Nb	Nt	Q	$Steady\ case$	$Unsteady\ case$
0.1	0.1	0.1	1.0	0.5787	1.0386
0.2				0.6186	1.0946
0.3				0.6571	1.1485
	0.1			0.5787	1.0386
	0.2			0.5392	0.9919
	0.3			0.5013	0.9469
		0.001		0.6031	1.0656
		0.05		0.5922	1.0535
		0.1		0.5787	1.0386
			0.1	1.0168	1.4133
			0.5	0.8219	1.2468
			1.0	0.5787	1.0386

Table 4. Results of Sherwood number $-\phi'(0)$ for various parameters

K	Nb	Nt	$Steady\ case$	$Unsteady\ case$
0.1	0.1	0.1	1.8553	1.4004
0.2			1.9876	1.5300
0.3			2.0219	1.7535
	0.1		1.6683	1.4568
	0.2		1.6766	1.5356
	0.3		1.6821	1.6248
		0.01	1.5138	1.6698
		0.05	1.5023	1.5620
		0.1	1.4149	1.4573

Table 5. Results of Motile density number $-h'(0)$ for various parameters

Lb	Pe	δ	$steady\ case$	$Unsteady\ case$
0.1	0.1	0.1	0.4213	0.4369
0.5			0.4473	0.5693
1.0			0.5373	0.6097
	0.1		0.5684	0.7064
	0.2		0.6289	0.7930
	0.3		0.8153	0.8437
		0.1	0.5358	0.7001
		0.2	0.5658	0.7283
		0.3	0.5963	0.7656

Conclusions

Unsteady Williamson nanofluid transport with mixed bioconvection across a rotating cone with porous wall is analysed numerically with an integrated effect of chemical reaction, heat generation/absorption and radiative heat transfer mechanisms. The governed system of non- linear differential equations are solved by computational procedure BVP5c technique with Matlab solver, and the following out comes of the key findings are:

- It is noted that when $\beta,\ Nr,\ Rb$ and $\Delta_u$uplift, the velocity $f'(\eta)$decreases. For Williamson parameter β, P, Δ_u effect the rate of change of motion of the liquid, it is initially increasing later on decrease in the x- direction as β, P, Δ_u rises.
- It is also evident that whenβ, m, and $\Delta_u$adopt greater values, the velocity$g'(0)$drops. Also, the rate of transfer of liquid motion is decrease first and at point of time liquid transfer increase gradually a for β, P, Δ_u rise.
- Thermal boundary layer thickness is decreases in the temperature profile when, $Ec, Nb, Nt, and\ R$ take bigger values. Conversely, when Pr rises temperature profile is decreasing. When heat absorption case, rate of heat transfer coefficient$-\theta'(0)$resulting in picture that the heat transfer rate is decreases initially after certain point the transfer rate is increases timely contrary behaviour shown for heat generation case
- it is evident that when $Nb, Sc,$ adopt greater values, the concentration profile $\phi(\eta)$ diminishes. When Nt rises, the concentration profile $\phi(\eta)$grows. Also mass transfer rate coefficient $\phi'(0)$ is increases for chemical reaction parameter K rises initially later on decreases gradually
- When $Lb, Pe, and\ \delta$ and take greater values, the motile density profile decreases.
- The Nusselt number increases when Q rises but decreases when $Nb, Nt,$ and Q take higher values.
- Sherwood number rises with elevated Sc, Nb, but for Nt rises mass transfer rate coefficient $-\phi'(0)$ increased in steady case where as decreased for unsteady case.
- As Lb, Pe, and δtake on greater values, the movable density number rises.

References:

[1] S. U. S. Choi, J. A. Eastman, and J. A. Eastman, “enhancing thermal conductivity of fluids with nanoparticles* enhancing thermal conductivity of fluids with nanoparticles,” 1935.

[2] F. Wang *et al.*, “The effects of nanoparticle aggregation and radiation on the flow of nanofluid between the gap of a disk and cone,” *Case Studies in Thermal Engineering*, vol. 33, May 2022, doi: 10.1016/j.csite.2022.101930.

[3] R. J. Punith Gowda, H. M. Baskonus, R. Naveen Kumar, B. C. Prasannakumara, and D. G. Prakasha, “Computational Investigation of Stefan

Blowing Effect on Flow of Second-Grade Fluid Over a Curved Stretching Sheet," *Int J Appl Comput Math*, vol. 7, no. 3, Jun. 2021, doi: 10.1007/s40819-021-01041-2.
[4] R. J. Punith Gowda *et al.*, "Thermophoretic particle deposition in time-dependent flow of hybrid nanofluid over rotating and vertically upward/ downward moving disk," *Surfaces and Interfaces*, vol. 22, Feb. 2021, doi: 10.1016/j.surfin.2020.100864.
[5] Y. X. Li *et al.*, "Dynamics of aluminium oxide and copper hybrid nanofluid in nonlinear mixed Marangoni convective flow with entropy generation: Applications to renewable energy," *Chinese Journal of Physics*, vol. 73, pp. 275–287, Oct. 2021, doi: 10.1016/j.cjph.2021.06.004.
[6] T. A. Yusuf, F. Mabood, B. C. Prasannakumara, and I. E. Sarris, "Magneto-bioconvection flow of Wlliamson nanofluid over an inclined plate with gyrotactic microorganisms and entropy generation," *Fluids*, vol. 6, no. 3, Mar. 2021, doi: 10.3390/fluids6030109.
[7] B. C. Prasannakumara, "Numerical simulation of heat transport in Maxwell nanofluid flow over a stretching sheet considering magnetic dipole effect," *Partial Differential Equations in Applied Mathematics*, vol. 4, Dec. 2021, doi: 10.1016/j.padiff.2021.100064.
[8] L. T. Benos, E. G. Karvelas, and I. E. Sarris, "A theoretical model for the magnetohydrodynamic natural convection of a CNT-water nanofluid incorporating a renovated Hamilton-Crosser model," *Int J Heat Mass Transfer*, vol. 135, pp. 548–560, Jun. 2019, doi: 10.1016/j.ijheatmasstransfer.2019.01.148.
[9] I. E. Sarris, S. Kassinos, B. Knaepen † A N, and D. D. Carati, "Large-eddy simulations of the turbulent Hartmann flow close to the transitional regime."
[10] E. Karvelas, C. Liosis, L. Benos, T. Karakasidis, and I. Sarris, "Micro mixing efficiency of particles in heavy metal removal processes under various inlet conditions," *Water (Switzerland)*, vol. 11, no. 6, Jun. 2019, doi: 10.3390/w11061135.
[11] R. J. Punith Gowda, R. Naveen Kumar, B. C. Prasannakumara, B. Nagaraja, and B. J. Gireesha, "Exploring magnetic dipole contribution on ferromagnetic nanofluid flow over a stretching sheet: An application of Stefan blowing," *J Mol Liq*, vol. 335, Aug. 2021, doi: 10.1016/j.molliq.2021.116215.
[12] R. J. Punith Gowda *et al.*, "Computational modelling of nanofluid flow over a curved stretching sheet using Koo–Kleinstreuer and Li (KKL) correlation and modified Fourier heat flux model," *Chaos Solitons Fractals*, vol. 145, Apr. 2021, doi: 10.1016/j.chaos.2021.110774.
[13] R. J. Punith Gowda, R. Naveen Kumar, A. M. Jyothi, B. C. Prasannakumara, and I. E. Sarris, "Impact of binary chemical reaction and activation energy on heat and mass transfer of Marangoni driven boundary layer flow of a non-Newtonian nanofluid," *Processes*, vol. 9, no. 4, Apr. 2021, doi: 10.3390/pr9040702.
[14] R. J. P. Gowda, R. N. Kumar, A. Rauf, B. C. Prasannakumara, and S. A. Shehzad, "Magnetized flow of Sutter by nanofluid through Cattaneo-Christov theory of heat diffusion and Stefan blowing condition," *Applied Nanoscience (Switzerland)*, vol. 13, no. 1, pp. 585–594, Jan. 2023, doi: 10.1007/s13204-021-01863-y.
[15] R. J. P. Gowda, A. Rauf, R. Naveen Kumar, B. C. Prasannakumara, and S. A. Shehzad, "Slip flow of Casson–Maxwell nanofluid confined through stretchable

disks," *Indian Journal of Physics*, vol. 96, no. 7, pp. 2041–2049, Jun. 2022, doi: 10.1007/s12648-021-02153-7.
[16] R.V. Williamson, "Literature Cited (1) Chipman," Industrial and Engineering chemistry, 1929.
[17] S. Abdal, I. Siddique, D. Alrowaili, Q. Al-Mdallal, and S. Hussain, "Exploring the magnetohydrodynamic stretched flow of Williamson Maxwell nanofluid through porous matrix over a permeated sheet with bioconvection and activation energy," *Sci Rep*, vol. 12, no. 1, Dec. 2022, doi: 10.1038/s41598-021-04581-1.
[18] S. Qayyum, M. I. Khan, F. Masood, Y. M. Chu, S. Kadry, and M. Nazeer, "Interpretation of entropy generation in Williamson fluid flow with nonlinear thermal radiation and first-order velocity slip," in *Mathematical Methods in the Applied Sciences*, John Wiley and Sons Ltd, Jun. 2021, pp. 7756–7765. doi: 10.1002/mma.6735.
[19] M. Waqas, M. Ijaz Khan, Z. Asghar, S. Kadry, Y. M. Chu, and W. A. Khan, "Interaction of heat generation in nonlinear mixed/forced convective flow of Williamson fluid flow subject to generalized Fourier's and Fick's concept," *Journal of Materials Research and Technology*, vol. 9, no. 5, pp. 11080–11086, 2020, doi: 10.1016/j.jmrt.2020.07.068.
[20] Y. M. Chu, U. Nazir, M. Sohail, M. M. Selim, and J. R. Lee, "Enhancement in thermal energy and solute particles using hybrid nanoparticles by engaging activation energy and chemical reaction over a parabolic surface via finite element approach," *Fractal and Fractional*, vol. 5, no. 3, Sep. 2021, doi: 10.3390/fractalfract5030119.
[21] Y. M. Chu *et al.*, "Combined impacts of heat source/sink, radiative heat flux, temperature dependent thermal conductivity on forced convective Rabinowitsch fluid," *International Communications in Heat and Mass Transfer*, vol. 120, Jan. 2021, doi: 10.1016/j.icheatmasstransfer.2020.105011.
[22] S. Abdal, I. Siddique, I. S. U. Din, A. Ahmadian, S. Hussain, and M. Salimi, "Significance of magnetohydrodynamic Williamson Sutterby nanofluid due to a rotating cone with bioconvection and anisotropic slip," *ZAMM Zeitschrift fur AngewandteMathematik und Mechanik*, vol. 102, no. 9, Sep. 2022, doi: 10.1002/zamm.202100503.
[23] U. Habib, S. Abdal, I. Siddique, and R. Ali, "A comparative study on micropolar, Williamson, Maxwell nanofluids flow due to a stretching surface in the presence of bioconvection, double diffusion and activation energy," *International Communications in Heat and Mass Transfer*, vol. 127, Oct. 2021, doi: 10.1016/j.icheatmasstransfer.2021.105551.
[24] A. U. Yahya, N. Salamat, D. Habib, B. Ali, S. Hussain, and S. Abdal, "Implication of Bio-convection and Cattaneo-Christov heat flux on Williamson Sutterby nanofluid transportation caused by a stretching surface with convective boundary," *Chinese Journal of Physics*, vol. 73, pp. 706–718, Oct. 2021, doi: 10.1016/j.cjph.2021.07.028.
[25] E. M. A. Elbashbeshy, N. T. M. Eldabe, I. K. Youssef, and A. M. Sedki, "Effects of pressure stress work and thermal radiation on free convection flow around a sphere embedded in a porous medium with Newtonian heating," *Thermal Science*, vol. 22, no. 1, pp. 401–412, 2018, doi: 10.2298/TSCI150601207E.

[26] M. A. Xenos, E. N. Petropoulou, A. Siokis, and U. S. Mahabaleshwar, "Solving the nonlinear boundary layer flow equations with pressure gradient and radiation," *Symmetry (Basel)*, vol. 12, no. 5, May 2020, doi: 10.3390/SYM12050710.
[27] A. J. Chamkha, A. M. Aly, and M. A. Mansour, "Similarity solution for unsteady heat and mass transfer from a stretching surface embedded in a porous medium with suction/injection and chemical reaction effects," *Chem Eng Commun*, vol. 197, no. 6, pp. 846–858, Jun. 2010, doi: 10.1080/00986440903359087.
[28] M. H. Matin and I. Pop, "Forced convection heat and mass transfer flow of a nanofluid through a porous channel with a first order chemical reaction on the wall," *International Communications in Heat and Mass Transfer*, vol. 46, pp. 134–141, Aug. 2013, doi: 10.1016/j.icheatmasstransfer.2013.05.001.
[29] C. Zhang, L. Zheng, X. Zhang, and G. Chen, "MHD flow and radiation heat transfer of nanofluids in porous media with variable surface heat flux and chemical reaction," *Appl Math Model*, vol. 39, no. 1, pp. 165–181, Jan. 2015, doi: 10.1016/j.apm.2014.05.023.
[30] D. Pal and G. Mandal, "Influence of thermal radiation on mixed convection heat and mass transfer stagnation-point flow in nanofluids over stretching/shrinking sheet in a porous medium with chemical reaction," *Nuclear Engineering and Design*, vol. 273, pp. 644–652, Jul. 2014, doi: 10.1016/j.nucengdes.2014.01.032.
[31] K. Ramesh, S. U. Khan, M. Jameel, M. I. Khan, Y. M. Chu, and S. Kadry, "Bioconvection assessment in Maxwell nanofluid configured by a Riga surface with nonlinear thermal radiation and activation energy," *Surfaces and Interfaces*, vol. 21, Dec. 2020, doi: 10.1016/j.surfin.2020.100749.
[32] Y. Q. Song *et al.*, "Applications of modified Darcy law and nonlinear thermal radiation in bioconvection flow of micropolar nanofluid over an off centered rotating disk," *Alexandria Engineering Journal*, vol. 60, no. 5, pp. 4607–4618, Oct. 2021, doi: 10.1016/j.aej.2021.03.053.
[33] U. Farooq, H. Waqas, M. I. Khan, S. U. Khan, Y. M. Chu, and S. Kadry, "Thermally radioactive bioconvection flow of Carreau nanofluid with modified Cattaneo-Christov expressions and exponential space-based heat source," *Alexandria Engineering Journal*, vol. 60, no. 3, pp. 3073–3086, Jun. 2021, doi: 10.1016/j.aej.2021.01.050.
[34] S. Abdal, I. Siddique, S. M. Eldin, M. Bilal, and S. Hussain, "Significance of thermal radiation and bioconvection for Williamson nanofluid transportation owing to cone rotation," *Sci Rep*, vol. 12, no. 1, Dec. 2022, doi: 10.1038/s41598-022-27118-6.
[35] S. Saleem and S. Nadeem, "Theoretical analysis of slip flow on a rotating cone with viscous dissipation effects," *Journal of Hydrodynamics*, vol. 27, no. 4, pp. 616–623, Oct. 2015, doi: 10.1016/S1001-6058(15)60523-6.
[36] A. J. Chamkha and A. Al-Mudhaf, "Unsteady heat and mass transfer from a rotating vertical cone with a magnetic field and heat generation or absorption effects," *International Journal of Thermal Sciences*, vol. 44, no. 3, pp. 267–276, Mar. 2005, doi: 10.1016/j.ijthermalsci.2004.06.005.
[37] W. Deebani, A. Tassaddiq, Z. Shah, A. Dawar, and F. Ali, "Hall effect on radiative Casson fluid flow with chemical reaction on a rotating cone through entropy optimization," *Entropy*, vol. 22, no. 4, Apr. 2020, doi: 10.3390/E22040480.

[38] M. Faiz *et al.*, "Multiple slip effects on time dependent axisymmetric flow of magnetized Carreau nanofluid and motile microorganisms," *Sci Rep*, vol. 12, no. 1, Dec. 2022, doi: 10.1038/s41598-022-18344-z.
[39] L. Ali, I. Siddique, N. Salamat, S. Hussain, and S. Abdal, "The significance of Magnetohydrodynamics sutterby nanofluid flow with concentration depending properties across stretching/ shrinking sheet and porosity," *Int J Mod Phys B*, vol. 36, no. 31, Dec. 2022, doi: 10.1142/S021797922250223X.
[40] S. Abdal *et al.*, "On Time-Dependent Rheology of Sutterby Nanofluid Transport across a Rotating Cone with Anisotropic Slip Constraints and Bioconvection," *Nanomaterials*, vol. 12, no. 17, Sep. 2022, doi: 10.3390/nano12172902.
[41] A. Mariam *et al.*, "Bioconvection attribution for effective thermal transportation of upper convicted Maxwell nanofluid flow due to an extending cylindrical surface," *Case Studies in Thermal Engineering*, vol. 34, Jun. 2022, doi: 10.1016/j.csite.2022.102062.
[42] I. S. Ud Din, I. Siddique, R. Ali, F. Jarad, S. Abdal, and S. Hussain, "On heat and flow characteristics of Carreau nanofluid and tangent hyperbolic nanofluid across a wedge with slip effects and bioconvection," *Case Studies in Thermal Engineering*, vol. 39, Nov. 2022, doi: 10.1016/j.csite.2022.102390.